Understanding the Role of Interface in Deformation Behavior of Additively Manufactured Bimetallic Structures of Pure Metals

Ali Afrouzian and Amit Bandyopadhyay*

W. M. Keck Biomedical Materials Research Laboratory

School of Mechanical and Materials Engineering

Washington State University, Pullman, Washington, 99164, USA.

*E-mail – amitband@wsu.edu

Abstract

Directed energy deposition (DED)-based additive manufacturing (AM) was employed to fabricate three distinct bimetallic compositions to understand the role interface for the deformation behavior of bimetallic structures under compressive loading. Commercially pure titanium (CP Ti) with a hexagonal closed packed (HCP) structure, nickel (Ni) with a face-centered cubic (FCC), and tantalum (Ta) with a body-centered cubic (BCC) structure were selected to understand the deformation behavior within the pure metals and damage accumulation at the bimetallic interface. By incorporating the combination of these materials, such as Ni-Ti, Ni-Ta, and Ta-Ti, we aimed to manufacture layered-base polycrystalline composite structures with FCC-HCP, FCC-BCC, and BCC-HCP crystal unit cells, respectively. In Ni-Ti and Ni-Ta bimetallic structures, it was determined that deformation is controlled by the Ni region, where the highest deflection occurs when Ni bulges out and makes lateral stress at the interface, resulting in crack initiation, propagation, and failure of the structure. Structural edges

were found to experience the highest deformation, prompting grain inclination towards the <111> crystal orientation, resulting in a favorable orientation for dislocation slip and a higher Taylor factor. However, strong interfacial bonding and similar Young's modulus between Ta and Ti altered the deformation mechanisms to twinning formation in the Ti region and observed buckling of the entire structure without significant failure at the interface.

Keywords: Bimetallic structures; Deformation behavior; Additive Manufacturing; Nickel; Titanium; Tantalum

1. Introduction

Layer-based multi-materials inspired by Nature, such as nacre and bone, have gained significant attention in biomedical, aerospace, and other industries due to their unique properties and versatile applications [1-4]. When two or more different metals with distinct properties are combined in multi-material structures, the resulting final composite takes advantage of constituent characteristics and forms unique property combinations – such as high toughness and strength, strong stability in a severely corrosive environment, or thermal and electrical conductivity [5-8]. DED-based additive manufacturing (AM) has emerged as a technique for fabricating multi-material components with simple and complex shapes [9-11]. In part, the properties of bimetallic structures are intimately linked to their unit cell crystal structure, which governs the arrangement of atoms in the crystal lattice; this influences the mechanical strength, thermal and electrical conductivity, and deformation mechanisms [12]. For instance, slip activation is limited in HCP crystal lattice materials such as titanium (Ti), with three active slip

systems that result in strain localization and the formation of long shear cracks [13].]. In comparison, BCC and FCC metals have more shear bands that present as stress relief sites [14]. However, slip is not the only deformation mechanism. Twinning is expected in the plastic deformation of HCP and FCC lattice metals with low stacking fault energies. It can also occur in BCC lattice metals under high strain rates and low temperatures [15, 16]. DED-processed samples are hypothesized to offer strong metallurgical bonding for bimetallic structures. However, the direct fabrication of dissimilar metals poses significant challenges, including microstructure inhomogeneity, non-uniform melting, and rapid cooling, which can influence mechanical properties [17]. In addition, due to the inherent differences in the coefficient of thermal expansion (CTE) of the two metals, bimetallic structures are susceptible to failure – such as interfacial cracking, delamination, and porosity within each metal [18-21].

There are multiple ways to reduce interfacial inherent residual stresses and reduce failures. As such, the fabrication of functionally graded structures of Inconel 625 and Stainless steel through sequential deposition via the fusion welding process was performed to improve the mechanical properties of bulk bimetallic structures [17, 22]. Another study used a third material as a diffusion barrier layer between dissimilar metals. The study formed a smooth intermetallic phase and coherent transition along the interface [19, 23, 24]. Onuike et al. considered niobium a diffusion barrier between Ti64 and SS410, forming FeNb and β-Ti+Nb without brittle intermetallic phases [24]. A compositionally graded interface is another approach to fabricating bimetallic structures of two metals with differing thermal properties [2, 25, 26]. Many studies have been conducted to optimize the manufacturing process of bimetallic structures to improve the build quality, eliminate intermetallic cracking, and enhance mechanical properties. However,

there is limited scientific evidence regarding the role of polycrystalline bimetallic structures and their mechanical properties. The scientific objective of this work is to understand the deformation behavior and damage accumulations under compressive loading for the unique combination of different metals in a bimetallic structure processed via DED-based AM. Ta offers biocompatibility and chemical resistance, which has been highly used in medical and hightemperature coating applications [27]. Multiple studies were performed to understand the deformation mechanisms of polycrystalline Ta and reported that {111} and {100} are the dominant orientations during quasi-static compression [28, 29]. However, active slip systems in BCC crystal structure remain controversial, and a deep understanding of deformation mechanisms is crucial for accurately predicting mechanical response [30]. Nickel-based superalloys have been widely used in aerospace turbine blades owing to high-temperature strength, excellent corrosion and oxidation resistance [31], and displayed preferential {111} crystallographic orientation with considerably low Schmid factor and multiple available slip systems [32]. For Ti, α -phase plays a critical role in the deformation behavior with {1010} as the dominant crystallographic orientation [13], which is widely used in aerospace and biomedical applications [33]. By understanding the intricate relationship between the crystal structures of polycrystalline materials and the properties of bimetallic structures, we can unlock new opportunities for designing materials for unique applications.

In this study, we proposed a method to investigate the influence of bimetallic interfaces of different unit cell crystal structures on the mechanical properties of layered-base structures inspired by natural materials and industrial applications and summarized in **Fig. 1**. To understand the effect of height volume fraction of Ni on the compression properties, we differing Ni-Ti

structures of FCC-HCP systems with varying layer thicknesses were produced. The samples are labeled with a numeric value representing the percentage of total height occupied by nickel. For example, if 40% of the total height of a bimetallic structure is composed of nickel, the sample is referred to as "40Ni". After performing the compression test, it was found that increasing the volume fraction of the Ni did not affect their mechanical properties. The sample with the smallest Ni thickness displayed the highest compressive strength. Additional volume fraction structures, such as Ni-Ta (FCC-BCC) and Ti-Ta (HCP-BCC) and bimetallic structures with 50% of overall height for each constituent, were printed for further evaluation. Compression tests and finite element analysis (FEA) were performed on all configurations to study the role of the interface on their compression behavior.

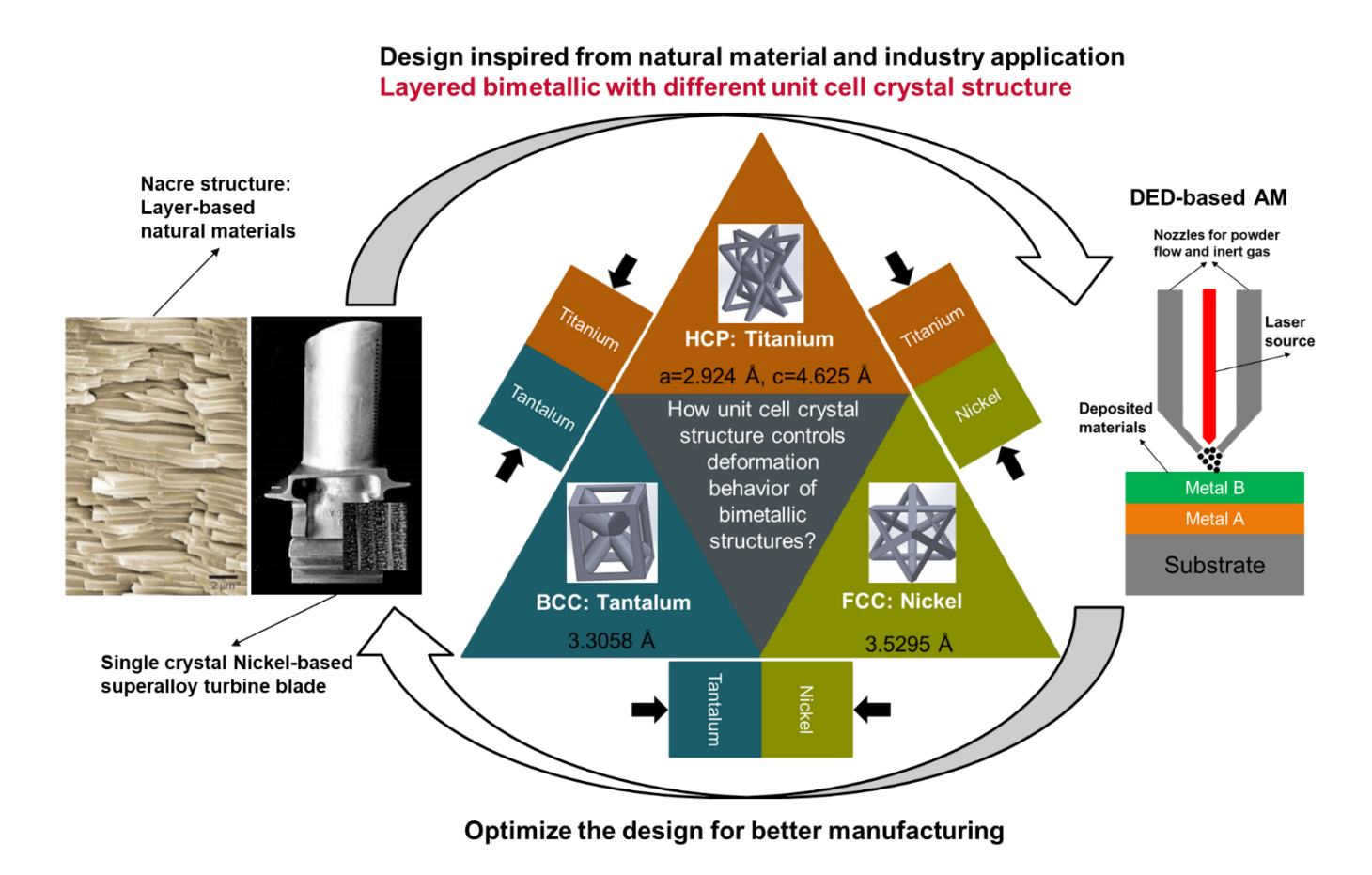


Figure 1. Nature and industry flow charts and Venn-style diagrams are used for inspiration in the current study [3, 7] for the fabrication of additively manufactured bimetallic structures, and they focus on the effect of their unit cell on bulk mechanical performance.

2. Materials and methods

2.1. Directed energy deposition - Processing of bimetallic structures

Spherical commercially pure Ti (Grade 2 Ancor-Ti, Hoganas, Sweden), nickel (Powder Alloy Corporation, Cincinnati, Ohio), and granular Ta (H.C. Stark, Newton, MA) powders with a particle size range of 45 – 150 µm were used in this study. The FormAlloy (Spring Valley, CA) DED system operates a 1000W laser to melt deposited powders onto a build plate connected to a stage that moves in the X/Y direction while the deposition head moves along the build in the Z

direction. The entire deposition head and build platform are enclosed in a controlled argon environment to keep the oxygen level below 15 ppm and avoid oxidation during the build process. Multiple prints were performed to reach optimized processing parameters. The processing parameters and compositions are summarized in **Table 1**.

Table 1 Processing Parameters of DED-fabricated Bimetallic Structures.

	Sample ID, thickness (t)(mm), number of layers (NOL)			Laser power (W)	Speed (mm/min)	Gas flow rate (l/min)		Powder feeder disc speed
Sample ID	IDs	t	NOL	C/H ²	C/H	Shield	Carrier	RPM
Ni-Ti ¹	Ni	0.3	11	420/450	800/750	18	14	0.5
	Ti	0.32	10	300/320	800/800	14	9	0.6
Ni-Ta	Ni	0.3	10	430/430	800/800	18	14	0.6
	Ta	0.2	15	450/450	800/750	15	11	0.7
Ta-Ti	Ti	0.32	10	430/450	800/800	14	9	0.5
	Ta	0.2	15	300/320	800/750	15	11	0.7

¹ It indicates 50% Ni- 50% Ti. Other combinations of Ni-Ti samples, such as 20Ni, were manufactured at different NOL according to each layer's thickness. As a result, 20% of the height belongs to Ni, and the rest belongs to Ti.

2.2. Phase analysis and microstructural characterization

XRD analysis was taken via a 40kV and 20mA Bruker D8 X-ray Diffractometer with Cu k-alpha radiation. There was a 2-D General Area Diffraction Detector mounted on a theta goniometer. The data were collected with an exposure time of 5 minutes/frame on the four sequential frames and were analyzed with Bruker DIFFRAC EVA software. Grinding (80–2000 grit SiC sandpaper) and polishing (1–0.05 µm alumina-DI water suspension) were performed for

 $^{^{2}}$ C = Contour, H = Hatch

the microstructure analysis, including Scanning Electron Microscopy (SEM, Ametek, PA). Kroll's solution (46 mL DI Water, 3 mL HNO3, & 1 mL HF) was used for Ti and Ni etching. To etch Ta, 10 g of NaOH was mixed with 100 mL of DI water, and the sample was immersed for 30 sec. One more polishing step was performed on the sample to get an excellent surface finish for the EBSD analysis. To this end, samples were also polished via a low nap cloth, electropolished in 0.02 colloidal silica suspension for 4 h at 2 V, and rinsed in ethanol immediately. EBSD was carried out with an accelerating voltage of 20 KeV with a step size lower than 1 µm. EBSD data were analyzed using a TSL orientation imaging microscopy (OIM Analysis version 7.0). The data was cleaned via neighbor grain CI standardization (CI > 0.05), and one-step grain dilation with approximately 5% of the data points adjustment.

2.3. FEM analysis and compression testing

To gain insights into the spatial and temporal evolution of local strain and stress of the bimetallic components during compression tests while minimizing the computational complexities and costs, two-dimensional (2D) axisymmetric Finite Element Method (FEM) simulations were conducted using the commercial ANSYS software. The sample size was taken from the actual samples of the tests. Quad elements with single integration points were used. Mesh refinements were performed to avoid hourglassing. Stress-strain plots were imported via code as multi-linear isotropic hardening to capture the actual behavior of each constituent under compressive load. Despite the efforts to optimize computational resources, limitations in hardware capabilities prevented the simulation of a complete compression test. However, the primary goal of this study was to investigate the initial formation of shear bands and stress distribution, which are crucial factors leading to stress propagation and, ultimately, failure in

bimetallic composite structures under compression. The bottom edge was fixed in all three translational degrees of freedom (DOF), while rotation was allowed to ensure realistic simulation conditions. Displacement was applied from the top edge at the same speed as the experiment, and the intermetallic boundary was tied through nodes. A quasi-static compression test (UTM-HYD Instron) was performed at a constant crosshead displacement rate of 1.3 mm/min. Three samples per configuration were ground to a 5. 1 ± 0.05 mm side length and height 10.1 ± 0.05 mm. Stress and strain were captured through the force-displacement data coming from the Instron machine during the test.

3. Result and discussion

Plentiful literature has been published on the possibility of manufacturing defect-free bimetallic structures by providing several methods – including sequential graded structures, functionally graded structures involving intermediate diffusion barrier sections, and compositionally graded structures [2, 5, 24, 34]. The focus of the current study was to couple two dissimilar metals while minimizing intermetallic phases and delamination at the interface. As mentioned, minimal research has looked into the crystallographic structure's influence on the mechanical response of bimetallic structures under compressive load. The primary goal of this study was to determine whether the mechanical properties, such as compressive strength and failure strain, are primarily influenced by the thickness of individual layers or the volume fraction of each constituent. To this end, multiple Ni-Ti as FCC-HCP bimetallic structures with varying Ni and Ti thicknesses were printed and tested. Additionally, the combination of other unit cell crystal structures was studied. The selection of Ta as a BCC metal is justified by its exceptional refractory properties and unique properties such as high-temperature strength,

biocompatibility, and high density. Furthermore, Ta was investigated with other metals in BCC-FCC (Ta-Ni) and BCC-HCP (Ta-Ti) structures.

3.1. Deformation behavior of Ni-Ti FCC-HCP crystal structures

The stress-strain plot for different Ni-Ti bimetallic structures is presented in Fig. 2A. As represented, the sample with a lower Ni volume fraction (20Ni) shows the highest compressive strengths and yield stress with 1287 ± 10 MPa, 731 ± 12 MPa, respectively. The composite samples, with higher volume fractions of nickel such as 40Ni, 50Ni, and 60Ni, behave very similarly to pure Ti. In the composite sample with the highest amount of nickel layers (80Ni), the compressive behavior is dominated by Ni, with an ultimate compressive strength of 420 ± 5 MPa. Moreover, strain hardening in 20Ni, 40Ni, 50Ni, and 60Ni is almost the same with a strain hardening exponent ~0.55, but in the 80Ni sample, it is around 0.49. Strain hardening of composite samples is attributed to the interface bonding and phase formation. For instance, in 20Ni with the smallest thickness of the nickel section, higher compressive strength and strain hardening were achieved. While with the addition of nickel thickness, strength is reduced. Phase formation at the interface of nickel and titanium can act as a strengthening mechanism when nickel thickness is small [33]. The 50Ni sample in **Fig. 2B** shows the Ni side bulged outwards, causing the Ti side to be stretched out, creating a transverse tensile stress. This stress contributes to the propagation of small cracks in the loading direction. Nickel with FCC crystal structure allows the easy movement of dislocations and can accommodate strain through dislocation glide and slip. As a result, it undergoes plastic deformation, leading to a bulging effect. However, titanium with an HCP crystal structure restricts the mobility of dislocation motion. The inability of titanium to accommodate strain through dislocation slip leads to stress concentration,

manifesting as observed cracking in the titanium section. In addition, the mismatch between the elastic modulus between nickel and titanium leads to the accumulation of stresses at the interface, acting as preferential sites for crack initiation in the titanium sites. In contrast, in the 20Ni composition, the thin layer of nickel does not bulge out to the extent of creating any tensile stress at the interface, resulting in smaller sites for crack formation in the titanium section and higher compressive strength. Quasi-static FEM simulation of the 50Ni sample showed the bulging effect on the Ni region and the onset of maximum von-mises stress at the interface, as the experiment predicted. Maximum principal strain accumulates to the nickel's center, leading to higher plastic deformation. This is intuitive due to Poisson's ratio of nickel and titanium. As such, Poisson's ratio to nickel is around 0.3, and Poisson's ratio to titanium is around 0.34. Higher Poisson's titanium ratio leads to lower lateral deformation, which leads to strain and stress mismatch at the interface. No crack initiation and propagation were seen in the FEM simulation, as failure criteria were not added to the simulation to control computational cost. The general behavior of the bimetallic structure and a comparison against experimental data are the main concepts of this work. Microstructural and elemental maps of the intermetallic region are presented in Fig. 2D. A gradient transition from acicular a-phase Ti to the equiaxed bimetallic part is seen with no cracking and porosity.

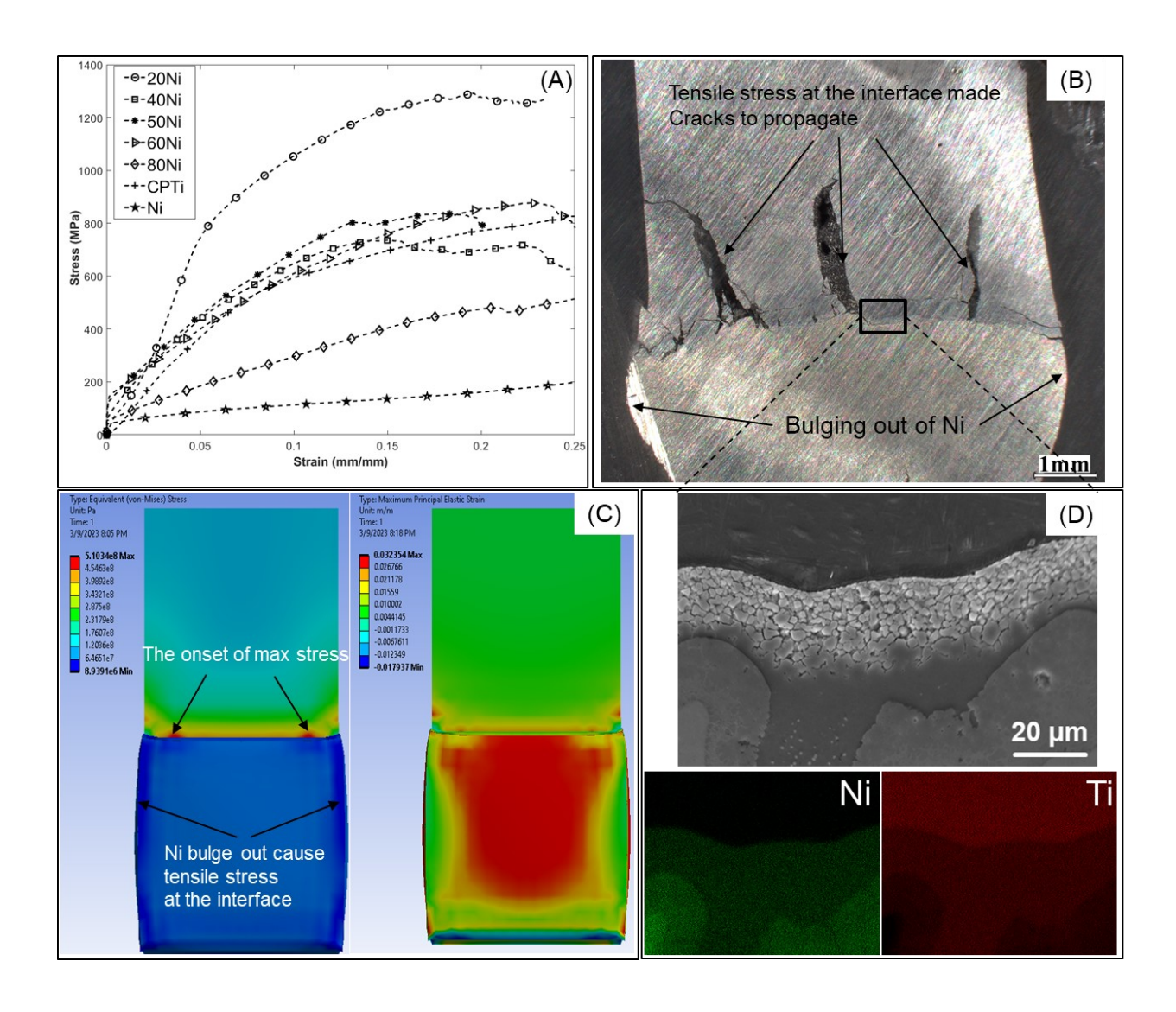


Figure 2. Deformation behavior for the Ni-Ti sample. (A) stress-strain plot for different compositions; (B) fracture surface from the cross-section of the 50Ni compressed sample; (C) FEA of the 50Ni; (D) SEM and EDS of the interface between Ni and Ti.

It is also discussed in previous work that there are austenite and martensite NiTi reactive phases formed at the reaction zone of the interface, while there is no nickel deposition in the titanium region [33]. High-temperature austenite B2 and low-temperature martensite B19' reactive phases formed during the cyclic heating and cooling, respectively. By going away from

the substrate, the cooling rate reduces, leading to the reduction of B2 phase at the interface of the bimetallic. However, the formation of NiTi phases, known for their hyperelastic and shape memory properties, influenced the mechanical properties of the bimetallic structures under compressive loading by providing crack-arresting ability.

EBSD figures, including grain map, grain size range, and inverse pole figure maps (IPF), are shown in **Fig. 3B** and **C**. The deformation in the Ni side is dominant and affects the whole compression behavior of the structure, so EBSD was taken from this region before and after the compression test. Ni has an FCC crystal structure, and the IPF map shows orientations of the grains towards forming the <001> plane parallel to the compression axis. After compression testing, the crystal structures rotated towards the <111> plane parallel to the compression axis. In polycrystalline materials, plasticity or material flow is considered to be a combination of many preferred crystallographic textures. The overall flow or yield stress (σ) of a polycrystal is similar to single crystals and can be represented in terms of critical resolved shear stress (τ_{crss}) and Taylor factor (M) according to the following equation [31]:

$$\sigma = \tau_{crss} M$$

According to this theory, the Taylor factor is the amount of work required to deform while all grains undergo identical strain. As a result, a higher Taylor factor represents a greater amount of work required to deform a grain, and lower strain values would be expected [31, 35, 36].

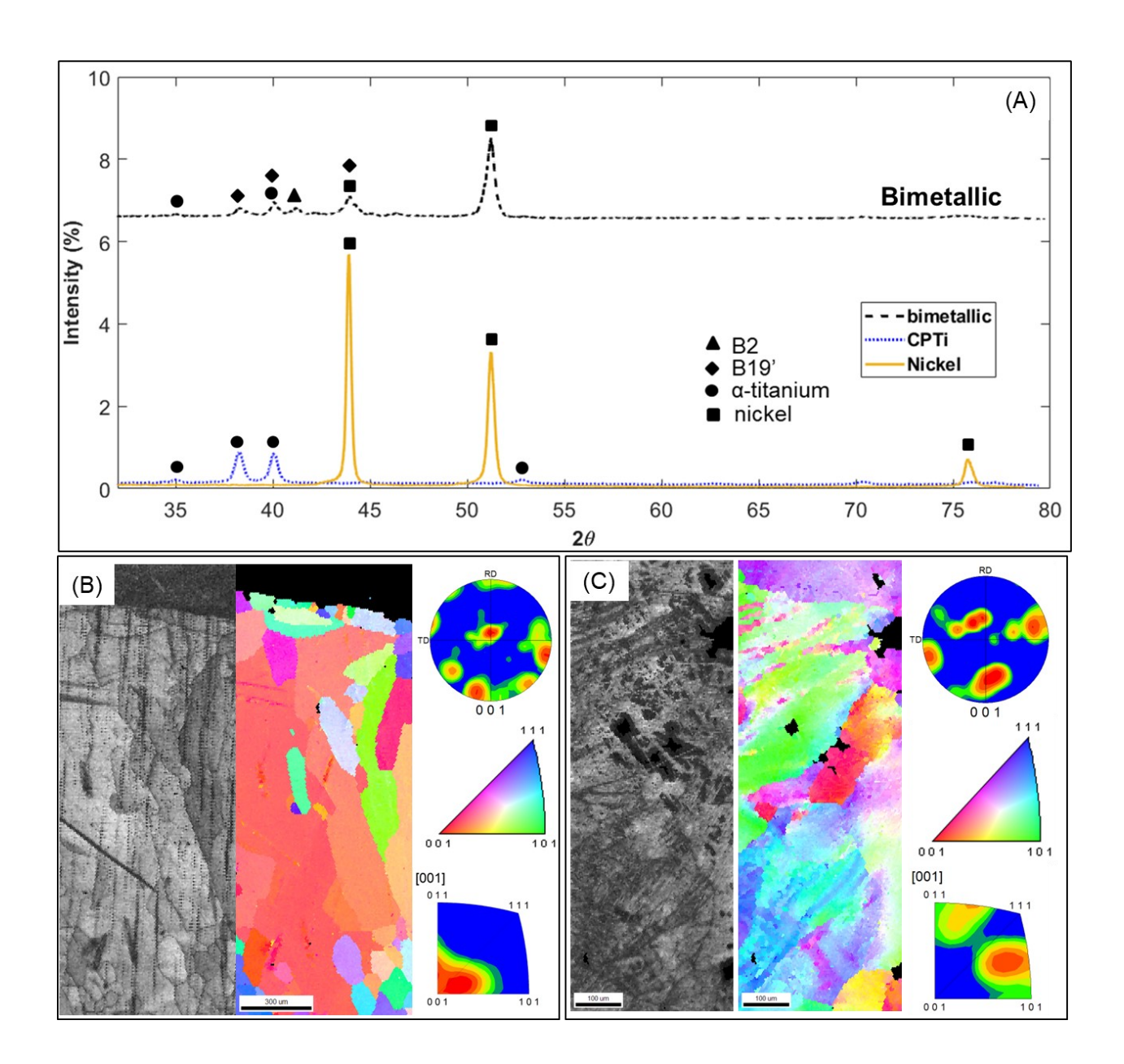


Figure 3. (A) XRD analysis of the Ni, Ti, and intermetallic region; (B) EBSD analysis of the asprinted specimen from the Ni region; (C) EBSD image for the compressed sample from the Ni region.

In further analysis, Taylor factors and inverse pole figures (IPF) for 20Ni and 50Ni specimens were captured and represented in Fig. 4. It is important to note that the rolling direction (RD) is considered to be in the build direction, and the sample was tilted 70 for the EBSD analysis. Load or unit strain tensor is also considered in the RD. In the Ni-Ti bimetallic sample, the Nickel region experienced the highest deformation. The EBSD images were, therefore, taken from the Ni region. Two main areas were selected for EBSD: close to the edge where most bulging occurred and in the middle section. Results show that the deformation of Ni is accomplished by dislocation slip and activation of the (111)[110] slip systems. These slip systems have the highest planar and linear density direction [33]. According to the IPF images in Fig. 4, middle section grains in the 50Ni sample are oriented mainly towards the <111> direction, and in the 20Ni sample <111> and <101> are the primary grain orientations. Closer to the edges, grains are mostly inclined towards the <001> direction in both compositions. Generally, the deformed metal of the edge section shows a higher Taylor factor than the nondeformed mid-section area. This is mainly because the preferred crystallographic orientation was acquired by plastic deformation that results in a more pronounced texture [31]. During compression, plastic deformation occurred most significantly at the edge of the nickel, causing nickel grains to elongate in the direction of maximum deformation. This leads to increased Taylor factor due to preferred orientation crystal lattice development.

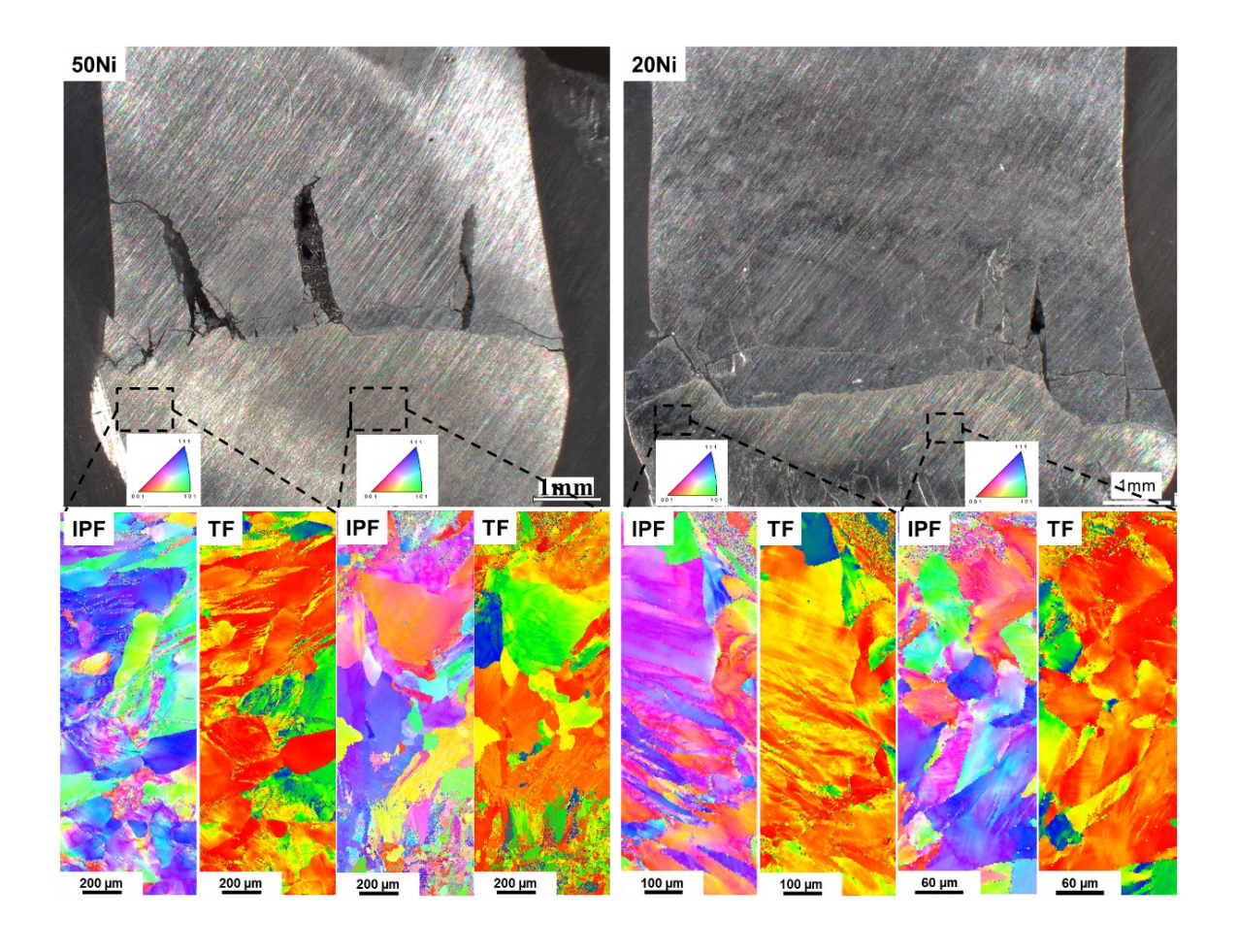


Figure 4. Inverse pole figure and Taylor factor maps of the mid and edge section of the bimetallic structures to <111> orientation for 50Ni-50Ti and 20Ni-80Ti.

3.2. Deformation behavior of Ni-Ta (FCC-BCC crystal structures)

Mechanical behavior, microstructural, and phase analysis of the Ni-Ta bimetallic are presented in **Fig 5**. The stress-strain plot of the nickel was discussed in the previous section. Pure polycrystalline tantalum with BCC crystal structure has 12 active slip systems, with higher deformation resistance than nickel with FCC crystal structure. This leads to more significant lattice distortion and crack initiation during the plastic deformation (**Fig 5B**). While pure tantalum showed a linear strain hardening behavior, Ni-Ta bimetallic exhibited a lower degree of

work hardening. Work hardening in polycrystalline tantalum is mainly due to the dislocation networks, which act like a barrier to the movement of additional dislocation, impeding further deformation [30]. Debonding at the interface is presented in Fig. 5B, while FEM captured the bulging effect resulting from higher lateral stress in Fig. 5C. Elastic lateral extension strain is proportional to the poison's ratio, and nominal stress and inverse of Young's modulus. Since Young's modulus of the Ni is lower than Ta, the lateral strain of the Ni is higher than the Ta. Additionally, plastic deformation preserves volume, so the Nickel bulges at the yielding region. Higher Von-Mises stress is recorded at the interface and bottom corners of the Ta section, gradually decreasing towards the upper layers of Ta. In addition, the elastic mismatch between tantalum and nickel and the DED process generate stresses and impurities, such as voids at the interface, that can facilitate crack nucleation. Unlike Ni-Ti bimetallic structures that formed a reactive phase at the interface with an effect on the mechanical properties of the bulk structures [33], there is no phase formation in the Ni-Ta bimetallic, according to the XRD plots in Fig. 5D. As a result, the stress distribution predicted by the FEM is governed by each of the components. In applying the load, a singularity developed at the corners. The higher Poisson's ratio of tantalum compared to nickel at the interface leads to a scenario where the Ni side experiences tangential tension, and the Ta side undergoes initial compression. When subjected to a nominal stress lower than its yield stress, Ni undergoes yielding, although Ta has significantly higher yielding stress (Fig 5A). The effective (plastic) Poisson's ratio of the material is approximately 0.5 during the plastic deformation. As a result, the stresses at the interface in Ta switch from compression to tension. This change in a stress state, combined with dislocation pileups in the Ni region that act as nucleation sites, leads to cracks in the Ta [37, 38]. EBSD images were taken from the middle and edge areas (Fig 5E and Fig 5F, respectively) of the Ni region since the

deformation is greater in this section. Nickel provides higher ductility and greater resistance to deformation compared to tantalum by accommodating plastic deformation through dislocation motion and slip with its FCC crystal structure. IPF maps show that the grains at the middle area are inclined towards the <001> crystal orientation, with rotation towards the <101> and <111> crystal orientation at the edge region. The compressed nickel experienced higher localized stress and strain (Fig. 5C), leading to a more intense deformation than the middle region.

Consequently, the middle section exhibits a higher Taylor factor than the edge region. A decreasing pattern is evident in the Taylor factor from top to bottom of Fig. 5F, which shows the edge region. The variation in Taylor factor values observed between the edge and middle regions of compressed nickel can be attributed to the influence of curvature and changes in deformation characteristics along the edge. Specifically, the curvature and deformation tend to decrease from the top to the bottom of the edge region. This behavior can be explained by the curvature's variations in the local strain distribution, causing more intense deformation near the top of the edge and gradually reducing strain towards the bottom.

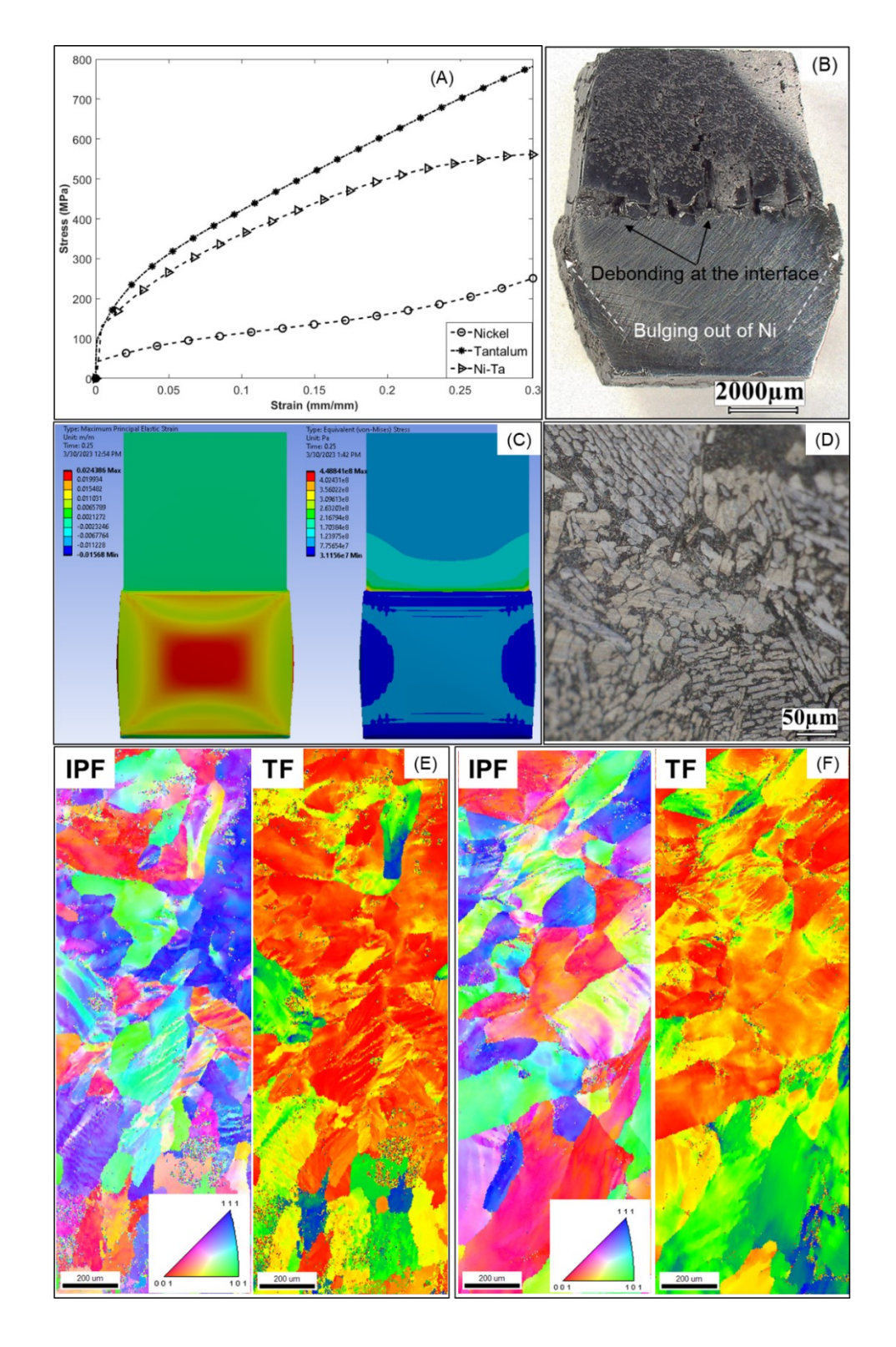


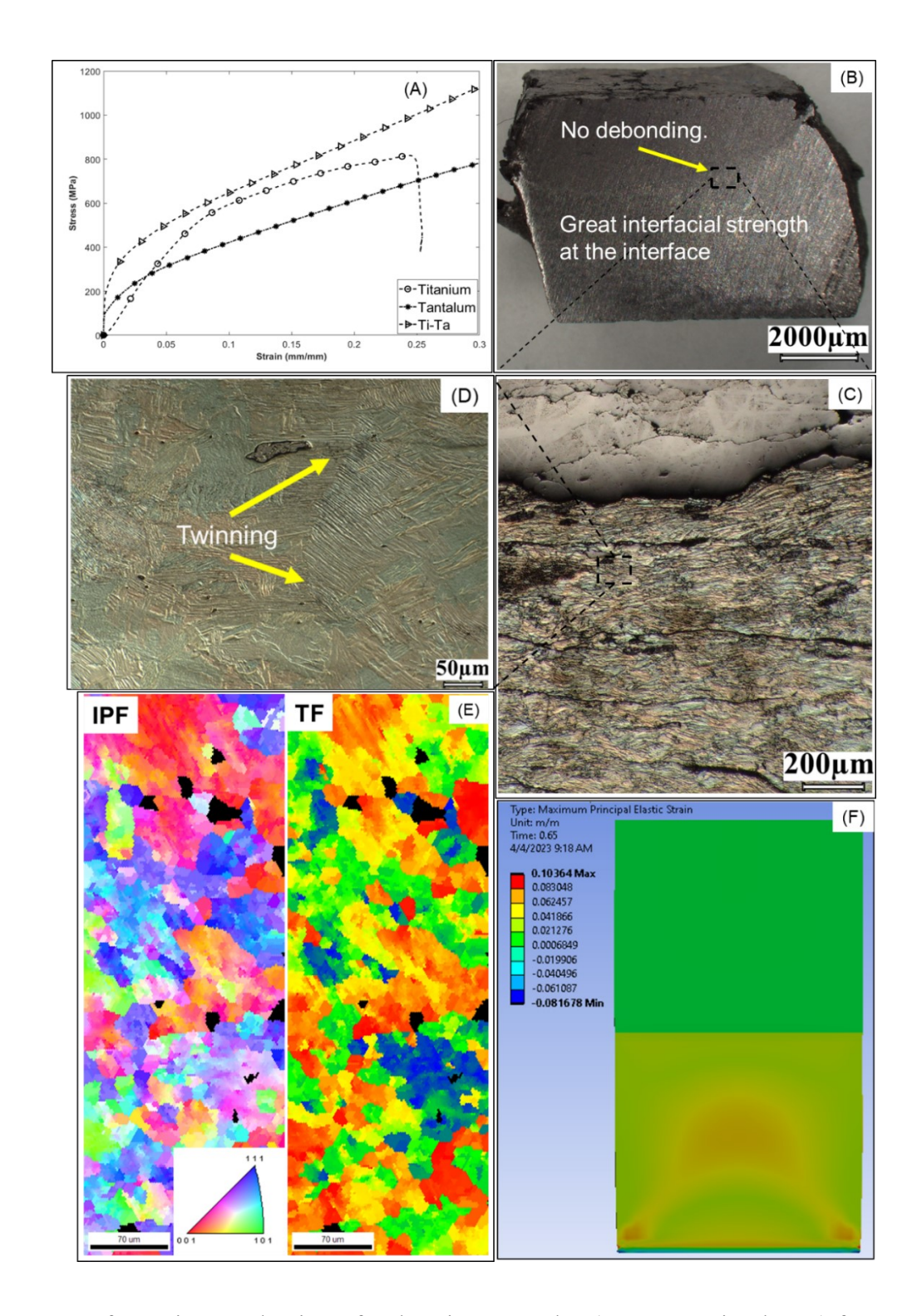
Figure 5. Deformation behavior for the Ni-Ta sample A) stress-strain plot, B) fractography from the cross-section of the compressed sample, C) FEA analysis, D) XRD spectra, and EBSD images of the compressed sample E) middle section, F) edge section.

3.3. Deformation behavior of Ti-Ta (HCP-BCC crystal structures)

Fig. 6 shows the mechanical response and characterization of the Ta-Ti bimetallic. Similar to the behavior observed in pure tantalum, our analysis of the Ta-Ti bimetallic structure reveals a notable enhancement in linear strain work hardening compared to each of the constituent materials [30]. This can be attributed to significant interfacial bonding at the interface (see Fig. 6B, C, and D) and the failure mechanisms characteristic of each metal. In other words, good metallurgical and mechanical compatibility between Ta and Ti resulted in a defect-free interface of the Ta-Ti bimetallic without any discontinuities and debonding at the interface. Ta acts as a β stabilizer phase in Ti during DED-based AM and promotes the retention of the β phase at lower temperatures, maintaining a higher proportion of this phase. This phenomenon can lead to strong interfacial bonding between two materials since the β phase of Ti often shows a higher strength and ductility [39, 40]. Great metallurgical and interfacial bonding between tantalum and titanium enhances the interface's mechanical integrity and load-carrying capacity. Titanium has an HCP crystal structure with three active slip systems, and as a result, twinning as another source of deformation was activated (Fig. 6C, D). Titanium has an HCP crystal structure with three active slip systems, and as a result, twinning as another source of deformation was activated (Fig. 6D). In Ti, since all of the slip directions are restricted to the basal plane, they cannot provide five independent slip systems to initiate plastic deformation and strain and deformation twinning becomes the dominant mechanisms in plastic deformation [41].

Interestingly, tantalum with BCC crystal structure tends to exhibit plastic deformation through dislocation motion and slip within its slip systems and crystal lattice, as presented in EBSD images in **Fig. 6E**. This leads to significant ductility and plasticity under compression.

Titanium and tantalum have almost the same Poisson ratio, and their Young's moduli are very close. The interface scan showed a similar pattern, but only Ti and Ta plots are represented in this study. Their lateral strain is supposed to be almost the same, leading to a smooth strain transition at the interface without debonding. According to FE analysis in **Fig. 6F**, there is no sharp strain transition at the interface or corners, which indicates good interfacial bonding. The close match in mechanical properties, such as Young's modulus, ensures an efficient stress transfer across the interface.



Figuew 6. Deformation mechanisms for the Ti-Ta sample A) stress-strain plot, B) fractography from the cross-section of the compressed sample, C and D) microstructure of the compressed Ta-Ti bimetallic and formation of twins in the Ti section, E) EBSD analysis of the edge of the tantalum side after compression, F) FEA analysis.

Compressive behavior and interface microstructural evolution is presented in Fig. 7. As presented, Ni-Ta showed the lowest compressive strength with a generated parabolic strain hardening. A sharp transition from needle-like grains in Ni to Ta makes this bimetallic susceptible to delamination sites at the interface. Especially, Ni with a higher number of closepacked active slip directions and lower Young's modulus showed higher lateral plastic strain and deformation, resulting in higher lateral tensile stress at the interface and formation of longitudinal cracks at the Ta region. This is the same mechanism in the Ni-Ti region as well. During the deformation, grains closer to the vertical edges in the Ni region can deform easily due to less restraint, and Ni bulges out [31]. However, grains at the mid-section of Ni did not experience any significant deformation or elongation and remained the same due to compressive stress in three directions. In Ta-Ti bimetallic representing the BCC-HCP interface junction, linear strain hardening is presented under a constant displacement control compression test. Smooth microstructural transition at the interface creates a relatively high local strain concentration area at the junctions [42]. Furthermore, the high-quality HCP-BCC interface that maintained its integrity at fracture resulted in deformation twinning at the Ti region.

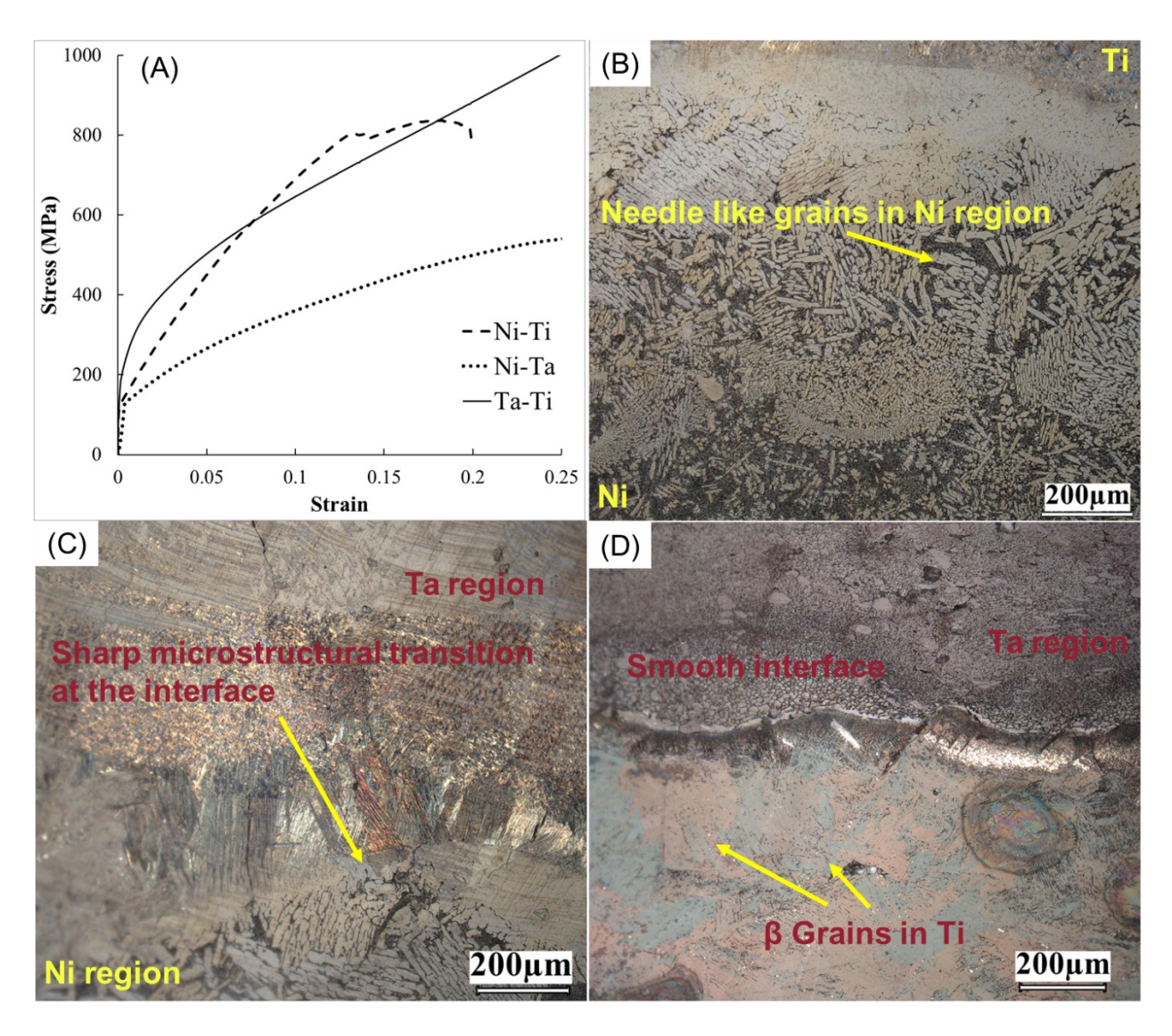


Figure 7 Deformation behavior of all bimetallic structures. (A) stress-strain plots, (B) Ni-Ti interface, (C) Ni-Ta interface, (D) Ta-Ti interface.

4. Conclusions

DED-based AM was used to understand the role of interfaces in the macroscale mechanical properties of bimetallic structures of pure metals. Bimetallic structures of CP Ti (HCP), Ni (FCC), and Ta (BCC) were processed as Ni-Ti, Ni-Ta, and Ta-Ti. This approach ensures that every potential pairing of the two components has been explored, enabling a

thorough investigation of their respective properties. All configurations were tested under quasistatic compression, and FEA and EBSD measurements were employed on the compressed samples to study the deformation and strengthening mechanisms of the bimetallic structures. It was found that Ni-Ti bimetallic sample, where both constituents have an equal height (50Ni sample), deformation primarily originates from the bulging effect of the Ni region. Before compression, the grains were predominantly oriented towards the <001> direction. However, a significant grain rotation towards the <111> direction was observed following compression, indicating a distinct reorientation of the crystal lattice in response to the applied force. In the composite with a lower number of Ni layers (20Ni), the relatively small thickness of the Ni layer influenced the bulk deformation behavior. Under compression loading in Ni-Ti and Ni-Ta samples, the plastic deformation of the nickel component exhibited the most notable occurrence at its edges. This localized deformation resulted in the elongation of nickel grains in the direction of maximum deformation. Consequently, a pronounced increase in the Taylor factor was observed, primarily due to the development of the preferred crystal lattice orientation. Finally, there was a strong interfacial bonding in Ta-Ti bimetallic structures, and twinning was the primary deformation mechanism in the Ti region.

5. Data Availability statement

The authors declare that all data supporting the findings of this study are available within the paper.

6. Acknowledgments

The authors would like to acknowledge financial support from the National Science Foundation under Grant Number CMMI 1934230. The authors would also like to acknowledge financial support from the JCDREAM (Seattle, WA) to acquire critical research equipment used in this work.

7. Conflict of Interest

None.

8. References

[1] H. D. Espinosa, A.L. Juster, F.J. Latourte, O.Y. Loh, D. Gregoire, P.D. Zavattieri, Tablet-level origin of toughening in abalone shells and translation to synthetic composite materials, Nat Commun 2 (2011) 173.

[2] B. E. Carroll, R.A. Otis, J.P. Borgonia, J.-o. Suh, R.P. Dillon, A.A. Shapiro, D.C. Hofmann, Z.-K. Liu, A.M. Beese, Functionally graded material of 304L stainless steel and inconel 625 fabricated by directed energy deposition: Characterization and thermodynamic modeling, Acta Materialia 108 (2016) 46-54.

[3] T. M. Pollock, Alloy design for aircraft engines, Nat Mater 15(8) (2016) 809-815.

[4] A. Bandyopadhyay, K. D. Traxel, S. Bose, Nature-inspired materials and structures using 3D Printing, Mater Sci Eng R Rep 145 (2021).

- [5] D. Gu, X. Shi, R. Poprawe, D.L. Bourell, R. Setchi, J. Zhu, Material-structure-performance integrated laser-metal additive manufacturing, Science 372(6545) (2021).
- [6] J. H. Martin, B.D. Yahata, J. M. Hundley, J. A. Mayer, T. A. Schaedler, T.M. Pollock, 3D printing of high-strength aluminium alloys, Nature 549(7672) (2017) 365-369.
- [7] U. G. Wegst, H. Bai, E. Saiz, A. P. Tomsia, R. O. Ritchie, Bioinspired structural materials, Nat Mater 14(1) (2015) 23-36.
- [8] C. Wei, L. Liu, Y. Gu, Y. Huang, Q. Chen, Z. Li, L. Li, Multi-material additive-manufacturing of tungsten copper alloy bimetallic structure with a stainless-steel interlayer and associated bonding mechanisms, Additive Manufacturing 50 (2022).
- [9] Y. Chen, S.J. Clark, D.M. Collins, S. Marussi, S.A. Hunt, D.M. Fenech, T. Connolley, R.C. Atwood, O.V. Magdysyuk, G.J. Baxter, M.A. Jones, C.L.A. Leung, P.D. Lee, Correlative Synchrotron X-ray Imaging and Diffraction of Directed Energy Deposition Additive Manufacturing, Acta Materialia 209 (2021).
- [10] P. Kurnsteiner, M.B. Wilms, A. Weisheit, B. Gault, E.A. Jagle, D. Raabe, High-strength Damascus steel by additive manufacturing, Nature 582(7813) (2020) 515-519.
- [11] X. Xie, J. Bennett, S. Saha, Y. Lu, J. Cao, W.K. Liu, Z. Gan, Mechanistic data-driven prediction of as-built mechanical properties in metal additive manufacturing, npj Computational Materials 7(1) (2021).
- [12] W. Zhang, Z. Ma, C. Li, C. Guo, D. Liu, H. Zhao, L. Ren, Micro/nano-mechanical behaviors of individual FCC, BCC and FCC/BCC interphase in a high-entropy alloy, Journal of Materials Science & Technology 114 (2022) 102-110.
- [13] J. Williams, R. Baggerly, N. Paton, Deformation behavior of HCP Ti-Al alloy single crystals, Metallurgical and Materials Transactions A 33 (2002) 837-850.

- [14] X. F. Tang, L.F. Peng, S.Q. Shi, M.W. Fu, Influence of crystal structure on size dependent deformation behavior and strain heterogeneity in micro-scale deformation, International Journal of Plasticity 118 (2019) 147-172.
- [15] X. Li, L. Lu, J. Li, X. Zhang, H. Gao, Mechanical properties and deformation mechanisms of gradient nanostructured metals and alloys, Nature Reviews Materials 5(9) (2020) 706-723.
- [16] X. Wang, J. Wang, Y. He, C. Wang, L. Zhong, S.X. Mao, Unstable twin in body-centered cubic tungsten nanocrystals, Nat Commun 11(1) (2020) 2497.
- [17] N. Chen, H.A. Khan, Z. Wan, J. Lippert, H. Sun, S.-L. Shang, Z.-K. Liu, J. Li, Microstructural characteristics and crack formation in additively manufactured bimetal material of 316L stainless steel and Inconel 625, Additive Manufacturing 32 (2020).
- [18] A. Bandyopadhyay, B. Heer, Additive manufacturing of multi-material structures, Materials Science and Engineering: R: Reports 129 (2018) 1-16.
- [19] L. D. Bobbio, B. Bocklund, R. Otis, J.P. Borgonia, R.P. Dillon, A.A. Shapiro, B. McEnerney, Z.-K. Liu, A.M. Beese, Characterization of a functionally graded material of Ti-6Al-4V to 304L stainless steel with an intermediate V section, Journal of Alloys and Compounds 742 (2018) 1031-1036.
- [20] D. C. Hofmann, S. Roberts, R. Otis, J. Kolodziejska, R.P. Dillon, J.O. Suh, A.A. Shapiro, Z.K. Liu, J.P. Borgonia, Developing gradient metal alloys through radial deposition additive manufacturing, Sci Rep 4 (2014) 5357.
- [21] B. Onuike, A. Bandyopadhyay, Bond Strength Measurement for Additively Manufactured Inconel 718- GRCop84 Copper Alloy Bimetallic Joints, Addit Manuf 27 (2019) 576-585.
- [22] M.R.U. Ahsan, X. Fan, G.-J. Seo, C. Ji, M. Noakes, A. Nycz, P.K. Liaw, D.B. Kim, Microstructures and mechanical behavior of the bimetallic additively-manufactured structure

- (BAMS) of austenitic stainless steel and Inconel 625, Journal of Materials Science & Technology 74 (2021) 176-188.
- [23] B. Onuike, A. Bandyopadhyay, Additive manufacturing of Inconel 718 Ti6Al4V bimetallic structures, Additive Manufacturing 22 (2018) 844-851.
- [24] B. Onuike, A. Bandyopadhyay, Functional Bimetallic Joints of Ti6Al4V to SS410, Addit Manuf 31 (2020).
- [25] Y. Zhang, A. Bandyopadhyay, Direct fabrication of compositionally graded Ti-Al2O3 multi-material structures using Laser Engineered Net Shaping, Additive Manufacturing 21 (2018) 104-111.
- [26] Y. Zhang, A. Bandyopadhyay, Influence of Compositionally Graded Interface on Microstructure and Compressive Deformation of 316L Stainless Steel to Al12Si Aluminum Alloy Bimetallic Structures, ACS Appl Mater Interfaces 13(7) (2021) 9174-9185.
- [27] T. DebRoy, H.L. Wei, J.S. Zuback, T. Mukherjee, J.W. Elmer, J.O. Milewski, A.M. Beese, A. Wilson-Heid, A. De, W. Zhang, Additive manufacturing of metallic components Process, structure and properties, Progress in Materials Science 92 (2018) 112-224.
- [28] Q. Zhu, Y. Liu, K. Song, Y. Zhou, X. Yang, S. Liu, Quasi-in-situ study on the crystallographic lattice rotation of tantalum during compression deformation, Journal of Materials Research and Technology 19 (2022) 858-865.
- [29] G. Whiteman, S. Case, J.C.F. Millett, M.J. Cox, P. Avraam, J.P. Dear, A. Sancho, P.A. Hooper, Uniaxial compression of single crystal and polycrystalline tantalum, Materials Science and Engineering: A 759 (2019) 70-77.

- [30] H. Lim, J.D. Carroll, J.R. Michael, C.C. Battaile, S.R. Chen, J.M. D. Lane, Investigating active slip planes in tantalum under compressive load: Crystal plasticity and slip trace analyses of single crystals, Acta Materialia 185 (2020) 1-12.
- [31] Q. Zhu, C. Wang, K. Yang, G. Chen, H. Qin, P. Zhang, Plastic deformation behavior of a nickel-based superalloy on the mesoscopic scale, Journal of Materials Science & Technology 40 (2020) 146-157.
- [32] C. P. Frick, B.G. Clark, S. Orso, A.S. Schneider, E. Arzt, Size effect on strength and strain hardening of small-scale [111] nickel compression pillars, Materials Science and Engineering: A 489(1-2) (2008) 319-329.
- [33] A. Afrouzian, C.J. Groden, D.P. Field, S. Bose, A. Bandyopadhyay, Additive manufacturing of Ti-Ni bimetallic structures, Materials & Design 215 (2022).
- [34] L. Yan, Y. Chen, F. Liou, Additive manufacturing of functionally graded metallic materials using laser metal deposition, Additive Manufacturing 31 (2020).
- [35] A. Harte, M. Atkinson, M. Preuss, J. Quinta da Fonseca, A statistical study of the relationship between plastic strain and lattice misorientation on the surface of a deformed Nibased superalloy, Acta Materialia 195 (2020) 555-570.
- [36] J. Jiang, T.B. Britton, A.J. Wilkinson, The orientation and strain dependence of dislocation structure evolution in monotonically deformed polycrystalline copper, International Journal of Plasticity 69 (2015) 102-117.
- [37] D. Bufford, Y. Liu, J. Wang, H. Wang, X. Zhang, In situ nanoindentation study on plasticity and work hardening in aluminium with incoherent twin boundaries, Nat Commun 5 (2014) 4864. [38] Y. Xu, S. Joseph, P. Karamched, K. Fox, D. Rugg, F.P.E. Dunne, D. Dye, Predicting dwell fatigue life in titanium alloys using modelling and experiment, Nat Commun 11(1) (2020) 5868.

- [39] D. Grevey, V. Vignal, I. Bendaoud, P. Erazmus-Vignal, I. Tomashchuk, D. Daloz, P. Sallamand, Microstructural and micro-electrochemical study of a tantalum–titanium weld interface, Materials & Design 87 (2015) 974-985.
- [40] Z. Liu, Z.B. Zhao, J.R. Liu, L. Wang, S.X. Zhu, G. Yang, S.L. Gong, Q.J. Wang, R. Yang, Deformation behaviors of as-built and hot isostatically pressed Ti-6Al-4V alloys fabricated via electron beam rapid manufacturing, Journal of Materials Science & Technology 35(11) (2019) 2552-2558.
- [41] A. A. Salem, S.R. Kalidindi, R.D. Doherty, Strain hardening of titanium: role of deformation twinning, Acta Materialia 51(14) (2003) 4225-4237.
- [42] M. Ardeljan, M. Knezevic, T. Nizolek, I.J. Beyerlein, N.A. Mara, T.M. Pollock, A study of microstructure-driven strain localizations in two-phase polycrystalline HCP/BCC composites using a multi-scale model, International Journal of Plasticity 74 (2015) 35-57.